

Indentation theory on orthotropic materials subjected to a frictional moving punch

Y. T. ZHOU¹), K. Y. LEE²), Y. H. JANG³)

¹) *School of Aerospace Engineering and Applied Mechanics
Tongji University
Shanghai 200092, People's Republic of China
e-mail: zhouyt@tongji.edu.cn*

²) *State Key Laboratory of Structural Analysis for Industrial Equipment
Department of Engineering Mechanics
Dalian University of Technology
Dalian 116024, People's Republic of China
e-mail: kylee@dlut.edu.cn*

³) *School of Mechanical Engineering
Yonsei University
Seoul 120-749, Republic of Korea*

THE PRESENT ARTICLE ESTABLISHES a general theory of frictional moving contact of orthotropic materials indented by a moving rigid punch with various punch profiles. The punch moves to the right or left at a constant speed with the shear stress arising inside the contact region. The motion should be subsonic. By using Galilean transformation and Fourier transform, a singular integral equation of the second kind is obtained, solution of which has a non-square-root or unconventional singularity. Numerical results are presented to show the influences of relative moving velocity and the friction coefficient on surface in-plane stress for each case of the four types of punches, which demonstrates that the surface crack initiation and propagation in load transfer components more likely occur at the trailing edge. The present theory provides a basis for explaining the surface damage mechanism of orthotropic materials under an indentation loading and for exploiting the physics behind the different punch profiles.

Key words: orthotropic materials, moving velocity, analytical solution, in-plane stress, surface crack.

Copyright © 2014 by IPPT PAN

1. Introduction

IN THE RECENT DECADE THERE HAS BEEN an increasing development of composite materials in many engineering applications, for example in construction sector. Because of the nature of the techniques used in processing, like the plasma spray technique [1] and electron beam physical vapor deposition method [2], the

composite materials are seldom isotropic. Thus, the inherent orthotropy should be considered and the mechanical behavior characteristics of orthotropic materials have been the subject of intense research. To accurately determine their mechanical properties is vital for orthotropic materials' applications.

Indentation techniques are ways to characterize material properties. Thus, the indentation problems have attracted attention of many engineers and scientists. For static indentation problems involving isotropic materials, a detailed description and review can be found in [3–6]. Studies of indentation problems in the non-isotropic materials were also considered. For early work about static contact problems of orthotropic materials, such as those presented by SVEKLO (1964 and 1970), WILLIS (1966), KIM and SUNCHELEEV (1970), one may refer to [4] (p. 579). SHI *et al.* [7] proposed a numerical method for the contact problem for orthotropic materials with the surface of the half-space parallel to two of the axes of material symmetry. SWANSON [8] showed how stresses and deformations can be determined throughout the contact region for an orthotropic half-space. Later, SWANSON [9] developed an approach to determine the entire stress, strain and deformation in orthotropic plates of finite thickness. In the above-mentioned papers involving contact mechanics, the punch indenting on the materials was stationary and the punch profiles were usually only flat-ended or round-ended. Besides, most results were given in numerical form.

Dynamic contact problem, in which a deformable half-space is indented by a moving rigid punch, is an important type of problem in contact mechanics and tribology [10] and has attracted researchers' attention. Using the plane-strain equations of linear elasticity, CRAGGS and ROBERTS [11] studied the moving of a heavy cylinder over the surface of an isotropic elastic half-space and obtained physically acceptable solutions for sub-Rayleigh and supersonic moving speeds. CLEMENT [12] extended results of CRAGGS and ROBERTS [11] to deal with the case when the cylinder is moving steadily over an anisotropic half-space. GEORGIADIS and BARBER [13] examined the elastodynamic super-Rayleigh/subseismic indentation paradox. BROCK [14] conducted a plane-strain analysis of steady sliding by a smooth rigid punch at any constant speed on a class of orthotropic or transversely isotropic half-spaces. These studies are frictionless. BABER and COMINON [15] studied the problem of an elastic cylinder rolling with friction on an elastic half-space with constant velocity which is supersonic with respect to the materials of the two bodies. Considering the presence of Coulomb friction, BROCK [16, 17] dealt with the steady-state sliding contact of thermoelastic half-spaces with only sub-Rayleigh speeds treated. Later, by allowing it to move with any (constant) speed (subsonic, transonic, and supersonic), BROCK and GEORGIADIS [18] treated friction-resisted sliding as a coupled thermoelastic process in the dynamic steady-state. The half-spaces, in the studies involving dynamic contact with friction, are isotropic and the

punch is either cylinder or saw-tooth. Using integral transforms and performing asymptotic analysis, BROCK and GEORGIADIS [19] addressed the frictional, dynamic steady state response of a coupled thermoelastic transversely isotropic half-space with multiple-zone, in which a complete solution was constructed for rounded “W”-shaped rigid indenter depicted by a fourth-order polynomial. Recently, ZHOU *et al.* [20] presented an exact contact analysis for orthotropic materials under a smoothly moving punch. Despite these work, more efforts need to be made to offer a deeper insight of how the punch profiles and the friction affect the dynamic contact between orthotropic materials and moving rigid punch with various punch profiles.

In this paper, a frictional moving contact model for orthotropic materials indented by a moving rigid punch with various punch profiles is established. The punch moves to the right or left at a constant speed and the motion should be subsonic. The complicated problem is reduced to singular integral equations of the second kind in terms of unknown contact stress under the punch. For four general punch profiles, such as a flat, triangular, parabolic or cylindrical profile, analytical solution of the reduced singular integral equations of the second kind is obtained, which may provide benchmark for the interpretation of the surface damage mechanism of general anisotropic materials under an indentation loading and the physics behind the different punch profiles. Numerical results show that the relative moving velocity c should be within the interval $[0, 1)$. The influences of relative moving velocity and the friction coefficient on surface in-plane stress are detailed. The present results show that the surface crack initiation and propagation in load transfer components are more likely to occur at the trailing edge.

2. Problem statement and boundary conditions

The problem under consideration consists of semi-infinite orthotropic materials in contact with a rigid punch. The stamp may possess various profiles. The punch moves frictionally to the right or left at a constant speed V , which should be not larger than the lowest bulk wave velocity as it will be mentioned later. Inside the contact region,

$$(2.1) \quad Q = \mu_f \cdot P,$$

where μ_f is the friction coefficient, P and Q are the resultant normal and tangential forces acting on the punch, respectively.

Plane strain state is considered. Stress components of the orthotropic materials can be written as

$$(2.2) \quad \begin{bmatrix} \sigma_{xx} \\ \sigma_{yy} \\ \tau_{xy} \end{bmatrix} = \begin{bmatrix} C_{11} & C_{12} & C_{13} \\ C_{21} & C_{22} & C_{23} \\ C_{31} & C_{32} & C_{33} \end{bmatrix} \begin{bmatrix} \partial u / \partial x \\ \partial v / \partial y \\ \partial u / \partial y + \partial v / \partial x \end{bmatrix},$$

where σ_{xx} , σ_{yy} and τ_{xy} are stress components, u and v are elastic displacements, and the elements C_{mn} are stiffness coefficients ($C_{13} = C_{23} = 0$, $C_{33} = G_0$).

Motion equations of free body forces are written as

$$(2.3) \quad \frac{\partial \sigma_{xx}}{\partial x} + \frac{\partial \tau_{xy}}{\partial y} = \rho \frac{\partial^2 u}{\partial t^2},$$

$$(2.4) \quad \frac{\partial \tau_{xy}}{\partial x} + \frac{\partial \sigma_{yy}}{\partial y} = \rho \frac{\partial^2 v}{\partial t^2},$$

where t is the time variable and ρ represents the mass density.

The Galilean transformation is introduced to make the time related problem tractable

$$(2.5) \quad X = x \mp Vt, \quad Y = y,$$

where “ $-$ ” denotes that the punch moves to the right, while “ $+$ ” to the left. The translating coordinate system (X, Y) is attached to the punch. In what follows, analyses will be conducted in the translating coordinate system (X, Y) .

In the coordinate system (X, Y) , the reduced problems are subjected to the following boundary conditions:

$$(2.6) \quad v(X, 0) = \begin{cases} -v_0, & X \in [-a, a], & \text{for flat,} \\ -v_0 + m_0 X, & X \in [0, b], & \text{for triangular,} \\ -v_0 + X^2 / (2R), & X \in [0, b], & \text{for parabolic,} \\ -v_0 + X^2 / (2R), & X \in [-a, b], & \text{for cylindrical,} \end{cases}$$

$$(2.7) \quad \sigma_{YY}(X, 0) = \begin{cases} -p(X), & X \in [-a, b], \\ 0, & X \notin [-a, b], \end{cases}$$

$$(2.8) \quad \tau_{XY}(X, 0) = \begin{cases} -q(X), & X \in [-a, b], \\ 0, & X \notin [-a, b], \end{cases}$$

where $v(X, 0)$ denotes the penetration depth, which is known a priori, $m_0 > 0$ and R is the radius of the parabolic or cylindrical punch. The surface stresses beneath the punch are unknown and are denoted by $p(X)$ and $q(X)$. In Eq. (2.6), the profile of the cylindrical punch is approximated as a parabola when $a + b \ll R$ [6]. The contact region and the physical nature at the edges of

the parabolic and cylindrical punch are quite different as it will be seen in Subsections 5.3 and 5.4. Equations (2.7) and (2.8) indicate that the contact stress and shear stress are unknown inside the contact region, while are free outside the contact region.

Inside the contact region, the Coulomb friction law applies, i.e.,

$$(2.9) \quad \tau_{XY}(X, 0) = \mu_f \sigma_{YY}(X, 0), \quad X \in [-a, b].$$

The equilibrium condition should be satisfied

$$(2.10) \quad \int_{-a}^b \sigma_{YY}(X, 0) dX = -P.$$

Note that in Eqs. (2.6)–(2.10), the contact region is denoted for convenience as $[-a, b]$ for various punch profiles.

Since the orthotropic materials are modeled as a semi-infinite plane, the displacements must vanish at infinity. Hence, one has

$$(2.11) \quad u(X, Y) \rightarrow 0, \quad v(X, Y) \rightarrow 0, \quad \sqrt{X^2 + Y^2} \rightarrow \infty.$$

3. Fundamental solutions

Substituting Eq. (2.2) into Eqs. (2.3) and (2.4) in view of Galilean transformation equation (2.5), one can get the governing equations, which have the following related characteristic equation:

$$(3.1) \quad \begin{vmatrix} -(C_{11} - C_{33} \cdot c^2) + C_{33}\eta^2 & -i \cdot \text{sgn}(\zeta) (C_{12} + C_{33}) \eta \\ -i \cdot \text{sgn}(\zeta) (C_{12} + C_{33}) \eta & -C_{33}(1 - c^2) + C_{22}\eta^2 \end{vmatrix} = 0,$$

where $\text{sgn}(\cdot)$ is the sign function and $i^2 = -1$.

Equation (3.1) is of quadratic order of η , in which only terms with even order of η remain. Considering regularity conditions equation (2.11), one may find that the eigenvalues of Eq. (3.1) take either of the following forms: (A) two pairs of complex conjugate roots (no purely imaginary roots) or (B) two pairs of opposite real roots. In what follows, eigenvectors $\Theta_n = [\Theta_{1n}(\zeta, Y) \ \Theta_{2n}(\zeta, Y)]^T$ ($n = 1, 2$) will be given for the each case of above eigenvalue distributions.

Case A: two pairs of complex conjugate roots (no purely imaginary roots)

$$(3.2) \quad \eta_1 = -\eta_4 = \theta + i \cdot \vartheta, \quad \eta_2 = -\eta_3 = \theta - i \cdot \vartheta,$$

where $\theta > 0$ and ϑ is a real number.

In this case, eigenvectors $\Theta_n = [\Theta_{1n}(\zeta, Y) \ \Theta_{2n}(\zeta, Y)]^T$ ($n = 1, 2$) are given by

$$(3.3) \quad \begin{aligned} \Theta_1 &= \begin{bmatrix} \cos(|\zeta| \vartheta Y) \\ -i \cdot \text{sgn}(\zeta) [\text{Re}(h(\eta_1)) \cos(|\zeta| \vartheta Y) - \text{Im}(h(\eta_1)) \sin(|\zeta| \vartheta Y)] \end{bmatrix} e^{|\zeta| \vartheta Y}, \\ \Theta_2 &= \begin{bmatrix} \sin(|\zeta| \vartheta Y) \\ -i \cdot \text{sgn}(\zeta) [\text{Im}(h(\eta_1)) \cos(|\zeta| \vartheta Y) + \text{Re}(h(\eta_1)) \sin(|\zeta| \vartheta Y)] \end{bmatrix} e^{|\zeta| \vartheta Y}, \end{aligned}$$

where $\text{Re}(\cdot)$ and $\text{Im}(\cdot)$ denote, respectively, the real part and imaginary part, and the function $h(\cdot)$ is defined as

$$(3.4) \quad h(\eta) = \frac{C_{33}\eta^2 - C_{11} + C_{33}c^2}{(C_{12} + C_{33})\eta}.$$

Case B: two pairs of opposite real roots

$$(3.5) \quad \eta_1 = -\eta_4 = \delta_1, \quad \eta_2 = -\eta_3 = \delta_2,$$

where $\delta_n > 0$ ($n = 1, 2$).

In this case, eigenvectors $\Theta_n = [\Theta_{1n}(\zeta, Y) \ \Theta_{2n}(\zeta, Y)]^T$ ($n = 1, 2$) are given by

$$(3.6) \quad \Theta_n = \begin{bmatrix} 1 \\ -i \cdot \text{sgn}(\zeta) h(\delta_n) \end{bmatrix} e^{|\zeta| \delta_n Y},$$

where $h(\cdot)$ is defined in Eq. (3.4).

Considering fundamental solutions given in Eq. (3.3) or (3.6) leads to the following expressions for the stresses:

$$(3.7) \quad \begin{bmatrix} \sigma_{XX}(X, Y) \\ \sigma_{YY}(X, Y) \\ \tau_{XY}(X, Y) \end{bmatrix} = \int_{-\infty}^{\infty} \sum_{n=1}^2 |\zeta| T_n \begin{bmatrix} \Omega_{1n}(\zeta, Y) \\ \Omega_{2n}(\zeta, Y) \\ \Omega_{3n}(\zeta, Y) \end{bmatrix} e^{-i\zeta X} d\zeta,$$

where T_n ($n = 1, 2$) are unknown functions to be determined from boundary conditions, and known functions $\Omega_{mn}(\zeta, Y)$ ($m = 1, 2, 3, n = 1, 2$) are given in Appendix.

Considering boundary conditions, one can determine unknown functions T_n ($n = 1, 2$). In the following section, integral equations will be established to determine unknown stresses $p(X)$ and $q(X)$ inside the contact region.

4. Integral equation

Differentiating the vertical displacement on the surface, one can obtain the following equation:

$$(4.1) \quad \frac{\partial v(X, 0)}{\partial X} = \frac{1}{\pi} \int_{-a}^b [K_1(X, v)p(v) + K_2(X, v)q(v)] dv.$$

Due to its role in causing surface damage, the surface in-plane stress can be given as

$$(4.2) \quad \sigma_{XX}(X, 0) = \frac{1}{\pi} \int_{-a}^b [L_1(X, v)p(v) + L_2(X, v)q(v)] dv.$$

The kernels $K_n(X, v)$ and $L_n(X, v)$ ($n = 1, 2$) in Eqs. (4.1) and (4.2) are given as

$$(4.3) \quad \begin{aligned} K_1(X, v) &= \int_0^\infty N_{11} \sin [\zeta (v - X)] d\zeta, \\ K_2(X, v) &= \int_0^\infty N_{12} \cos [\zeta (v - X)] d\zeta, \\ L_1(X, v) &= \int_0^\infty N_{21} \cos [\zeta (v - X)] d\zeta, \\ L_2(X, v) &= \int_0^\infty N_{21} \sin [\zeta (v - X)] d\zeta, \end{aligned}$$

where N_{mn} ($m, n = 1, 2$) are given as

$$(4.4) \quad \begin{aligned} N_{11} &= \sum_{n=1}^2 (-1)^n M_{n1} \Theta_{2n}(\zeta, 0), \\ N_{12} &= i \sum_{n=1}^2 (-1)^n M_{n2} \Theta_{2n}(\zeta, 0), \\ N_{21} &= \sum_{n=1}^2 (-1)^n M_{n1} \Omega_{1n}(\zeta, 0), \\ N_{22} &= i \sum_{n=1}^2 (-1)^{n+1} M_{n2} \Omega_{1n}(\zeta, 0), \end{aligned}$$

which are independent of ζ and M_{mn} ($m, n = 1, 2$) are given in Appendix.

Equations (4.1) and (4.2) can be rewritten as:

$$(4.5) \quad \frac{\partial v(X, 0)}{\partial X} = N_{12} \cdot \mu_f \cdot p(X) + \frac{1}{\pi} \int_{-a}^b \frac{N_{11}}{v - X} p(v) dv,$$

$$(4.6) \quad \sigma_{XX}(X, 0) = N_{21} p(X) + \frac{1}{\pi} \int_{-a}^b \frac{N_{22} \cdot \mu_f}{v - X} p(v) dv.$$

To obtain solutions of Eqs. (4.5) and (4.6), the following formulas are used:

$$(4.7) \quad \int_0^\infty \sin[\zeta(v - X)] d\zeta = \frac{1}{v - X}, \quad \int_0^\infty \cos[\zeta(v - X)] d\zeta = \pi \cdot \delta(v - X),$$

where $\delta(\cdot)$ is the Dirac delta function.

As mentioned above, the penetration depth $v(X, 0)$ is known a priori. Thus, the unknown function $p(X)$ can be solved from the Cauchy singular integral equation of the second type, i.e., Eq. (4.5), plus equilibrium condition Eq. (2.10). Equations (4.5) and (2.10) can be normalized as

$$(4.8) \quad N_{12} \cdot \mu_f \cdot \psi(s) + \frac{1}{\pi} \int_{-1}^1 \frac{N_{11}}{t - s} \psi(t) dt = \Lambda(s), \quad |s| < 1,$$

$$(4.9) \quad \int_{-1}^1 \psi(s) ds = \frac{2P}{b + a},$$

where the following changes of variable are used:

$$(4.10) \quad X = \frac{b + a}{2}s + \frac{b - a}{2}, \quad v = \frac{b + a}{2}t + \frac{b - a}{2}, \quad -a < (X, v) < b, \\ -1 < (s, t) < 1, \quad p(X) = \psi(s), \quad \frac{\partial v(X, 0)}{\partial X} = \Lambda(s).$$

To solve Eqs. (4.8) and (4.9), the following expression [21] is defined:

$$(4.11) \quad \Psi(z) = \frac{1}{2\pi i} \int_{-1}^1 \frac{\psi(t)}{t - z} dt,$$

which satisfies the following properties, i.e., general Plemelj formulae:

$$(4.12) \quad \Psi^+(s) - \Psi^-(s) = \begin{cases} \psi(s), & |s| < 1, \\ 0 & |s| > 1, \end{cases}$$

$$(4.13) \quad \Psi^+(s) + \Psi^-(s) = \begin{cases} \frac{1}{\pi i} \int_{-1}^1 \frac{\psi(t)}{t-s} dt, & |s| < 1, \\ 2\psi(s), & |s| > 1, \end{cases}$$

where superscripts ‘+’ and ‘-’ represent, respectively, the limits of $\Psi(z)$. With these relations, Eq. (4.8) can be written as the following Riemann–Hilbert problem:

$$(4.14) \quad A\Psi^+(s) = B\Psi^-(s) + \Lambda(s),$$

where

$$(4.15) \quad A = N_{12} \cdot \mu_f + N_{11} \cdot i, \quad B = N_{12} \cdot \mu_f - N_{11} \cdot i.$$

Considering the corresponding homogeneous equation of Eq. (4.14), one may find that the fundamental function that characterizes the nature of the contact stress is the weight function of Jacobi polynomials [22]

$$(4.16) \quad \varpi(s) = (1-s)^\alpha(1+s)^\beta, \quad |s| < 1.$$

As a result, the solution to the singular integral equation can be expressed in terms of the series expansion such that [23]

$$(4.17) \quad \psi(s) = \varpi(s) \sum_{j=0}^{\infty} c_j P_j^{(\alpha,\beta)}(s), \quad |s| < 1,$$

where $c_j (j \geq 0)$ are unknown coefficients to be determined, $P_j^{(\alpha,\beta)}(s)$ are Jacobi polynomials, and

$$(4.18) \quad \begin{aligned} \alpha &= -\frac{\varepsilon}{\pi} + N_0, & \beta &= \frac{\varepsilon}{\pi} + M_0, \\ \varepsilon &= \arctan\left(\frac{1}{\xi}\right), & \xi &= \frac{\mu_f N_{12}}{N_{11}}, \end{aligned}$$

where N_0 and M_0 are arbitrary integrals depending on the physics of the problem.

Substituting Eq. (4.17) into Eq. (4.8) and considering the following property of Jacobi polynomials:

$$(4.19) \quad \begin{aligned} N_{12} \cdot \mu_f \cdot P_j^{(\alpha,\beta)}(s) \cdot \varpi(s) + \frac{1}{\pi} \int_{-1}^1 \frac{N_{11}}{t-s} P_j^{(\alpha,\beta)}(t) \varpi(t) dt \\ = -2^{-\kappa_0} \frac{N_{11}}{\sin(\pi\tau)} P_{j-\kappa_0}^{(-\alpha,-\beta)}(s), \end{aligned}$$

where the index is $\kappa_0 = -(\alpha + \beta)$, one can obtain that

$$(4.20) \quad \sum_{j=0}^{\infty} c_j \left[-2^{-\kappa_0} \frac{N_{11}}{\sin(\pi\alpha)} P_{j-\kappa_0}^{(-\alpha, -\beta)}(s) \right] = \Lambda(s), \quad |s| < 1.$$

By expanding $\Lambda(s)$ in terms of Jacobi polynomials and comparing both sides of Eq. (4.20), the unknown coefficients c_j ($j \geq 0$) can be determined. Once the contact stress $p(X)$ is obtained, the in-plane stress on the surface can be evaluated by Eq. (4.6). In what follows, analytical solutions of the singular integral equation obtained above will be given for punches with various profiles.

5. Analytical solutions

5.1. For a frictional flat punch

Considering the first expression on the left-hand side of Eq. (2.6) and noting that $b = a$, one can rewrite Eqs. (4.8) and (4.9) as

$$(5.1) \quad N_{12} \cdot \mu_f \cdot \psi(s) + \frac{1}{\pi} \int_{-1}^1 \frac{N_{11}}{t-s} \psi(t) dt = 0, \quad |s| < 1,$$

$$(5.2) \quad \int_{-1}^1 \psi(s) ds = \frac{P}{a}.$$

At both edges $X = a$ and $X = -a$, the function $p(X)$ has integrable singularities, which require that both α and β be negative. By letting $N_0 = 0$ and $M_0 = -1$, α and β defined in Eq. (4.18) can be written as

$$(5.3) \quad \begin{aligned} \xi > 0: \quad \alpha &= -\frac{\xi}{\pi}, & \beta &= \frac{\xi}{\pi} - 1, \\ \xi = 0: \quad \alpha &= -\frac{1}{2}, & \beta &= -\frac{1}{2}, \\ \xi < 0: \quad \alpha &= \frac{\xi}{\pi} - 1, & \beta &= -\frac{\xi}{\pi}. \end{aligned}$$

Thus, the index κ_0 in this case is

$$(5.4) \quad \kappa_0 = -(\alpha + \beta) = 1.$$

Substituting Eq. (4.17) into Eqs. (5.1) and (5.2), and using Eq. (4.20) and the relation

$$(5.5) \quad \int_{-1}^1 \varpi(s) ds = \frac{2^{\alpha+\beta+1} \Gamma(\alpha+1) \Gamma(\beta+1)}{\Gamma(\alpha+\beta+2)},$$

where $\Gamma(\cdot)$ is the Gamma function, one can obtain the only nonzero coefficient c_0 as follows:

$$(5.6) \quad c_0 = -\frac{2P_0 \sin(\pi\alpha)}{\pi},$$

where

$$(5.7) \quad P_0 = \frac{P}{2a}.$$

Then, considering Eqs. (4.17), (4.10) and (2.7), one can get the surface normal stress as

$$(5.8) \quad \sigma_{YY}(X, 0) = \frac{2P_0 \sin(\pi\alpha)}{\pi} \left(1 - \frac{X}{a}\right)^\alpha \left(1 + \frac{X}{a}\right)^\beta, \quad |X| < a.$$

With consideration of Eqs. (5.8) and (2.7), the surface in-plane stress given in Eq. (4.6) can be rewritten in the following closed-form in terms of elementary functions:

$$(5.9) \quad \sigma_{XX}(X, 0) = -\frac{2P_0 \sin(\pi\alpha)}{\pi} \begin{cases} N_{21} \left(1 - \frac{X}{a}\right)^\tau \left(1 + \frac{X}{a}\right)^\vartheta + \frac{N_{22} \cdot \mu_f}{\pi} \Upsilon_f(X), & |X| < a, \\ \frac{N_{22} \cdot \mu_f}{\pi} \Upsilon_f(X), & |X| > a, \end{cases}$$

where $\Upsilon_f(X)$ is given as

$$(5.10) \quad \Upsilon_f(X) = \frac{\pi}{\sin(\pi\alpha)} \begin{cases} -\left(1 - \frac{X}{a}\right)^\alpha \left(-\frac{X}{a} - 1\right)^\beta, & X < -a, \\ \left(1 - \frac{X}{a}\right)^\alpha \left(1 + \frac{X}{a}\right)^\beta \cos(\pi\alpha), & -a < X < a, \\ \left(\frac{X}{a} - 1\right)^\alpha \left(1 + \frac{X}{a}\right)^\beta, & X > a. \end{cases}$$

The mode I stress intensity factors at the edges of the flat punch are defined as

$$(5.11) \quad F_I(a) = \lim_{X \rightarrow a} \frac{p(X)}{2^\beta} (a - X)^{-\alpha} = \frac{c_0}{a^\alpha},$$

$$(5.12) \quad F_I(-a) = \lim_{X \rightarrow -a} \frac{p(X)}{2^\alpha} (a + X)^{-\beta} = \frac{c_0}{a^\beta}.$$

In Eqs. (5.11) and (5.12), letting $\mu_f = 0$ leads to the following expression:

$$(5.13) \quad F_I(a) = F_I(-a) = c_0 \sqrt{a} = \frac{P}{\pi \sqrt{a}}.$$

5.2. For a frictional triangular punch

Considering the second expression on the left-hand side of Eq. (2.6) and noting that $a = 0$, one can rewrite Eqs. (4.8) and (4.9) as

$$(5.14) \quad N_{12} \cdot \mu_f \cdot \psi(s) + \frac{1}{\pi} \int_{-1}^1 \frac{N_{11}}{t-s} \psi(t) dt = m_0, \quad |s| < 1,$$

$$(5.15) \quad \int_{-1}^1 \psi(s) ds = \frac{2P}{b}.$$

In this case, α is positive and β is negative since the triangular punch has a sharp corner at $X = 0$ and smooth contact at $X = b$. By letting $N_0 = 1$ and $M_0 = -1$, α and β defined in Eq. (4.18) can be presented as:

$$(5.16) \quad \begin{aligned} \xi > 0 : \quad \alpha &= 1 - \frac{\varepsilon}{\pi}, & \beta &= -1 + \frac{\varepsilon}{\pi}, \\ \xi = 0 : \quad \alpha &= \frac{1}{2}, & \beta &= -\frac{1}{2}, \\ \xi < 0 : \quad \alpha &= \frac{\varepsilon}{\pi}, & \beta &= -\frac{\varepsilon}{\pi}. \end{aligned}$$

Thus, the index κ_0 in this case is

$$(5.17) \quad \kappa_0 = -(\alpha + \beta) = 0.$$

Substituting Eq. (4.17) into Eq. (5.14), using Eq. (4.20) and considering Eq. (5.5) produce the only nonzero coefficient c_0 as follows:

$$(5.18) \quad c_0 = \frac{m_0 \cdot \sin(\pi\alpha)}{-N_{11}}.$$

Then, considering Eqs. (4.17), (4.10) and (2.7), one can get the surface normal stress as

$$(5.19) \quad \sigma_{YY}(X, 0) = \frac{m_0}{N_{11}} \cdot \sin(\pi\alpha) \cdot \left(\frac{b-X}{X} \right)^\alpha, \quad 0 < X < b.$$

The surface in-plane stress given Eq. (4.6) can be rewritten in the following closed-form:

$$(5.20) \quad \begin{aligned} &\sigma_{XX}(X, 0) \\ &= \frac{m_0}{-N_{11}} \cdot \sin(\pi\alpha) \begin{cases} N_{21} \left(\frac{b-X}{X} \right)^\alpha + \frac{N_{22} \cdot \mu_f}{\pi} \gamma_t(X), & 0 < X < b, \\ \frac{N_{22} \cdot \mu_f}{\pi} \gamma_t(X), & X \notin [0, b], \end{cases} \end{aligned}$$

where $\mathcal{Y}_t(X)$ is given as

$$(5.21) \quad \mathcal{Y}_t(X) = \frac{\pi}{\sin(\pi\alpha)} \begin{cases} \left(\frac{X-b}{X}\right)^\alpha - 1, & X < 0, \\ \left(\frac{b-X}{X}\right)^\alpha \cos(\pi\alpha) - 1, & 0 < X < b, \\ \left(\frac{X-b}{X}\right)^\alpha - 1, & X > b. \end{cases}$$

Besides, substituting Eq. (4.17) into Eq. (5.15) in view of Eqs. (5.18) and (4.16) yields the following formula to determine the contact length:

$$(5.22) \quad b = \frac{-N_{11} \cdot P}{m_0 \cdot \pi \cdot \alpha}.$$

The mode I stress intensity factor at the leading edge of the triangular punch can be defined as follows:

$$(5.23) \quad k_1(0) = \lim_{X \rightarrow 0} X^\alpha p(X) = \frac{m_0 \cdot \sin(\pi\alpha) \cdot b^\alpha}{-N_{11}}.$$

5.3. For a frictional parabolic punch

Considering the third expression on the left-hand side of Eq. (2.6) and noting that $a = 0$, one can rewrite Eqs. (4.8) and (4.9) as

$$(5.24) \quad N_{12} \cdot \mu_f \cdot \psi(s) + \frac{1}{\pi} \int_{-1}^1 \frac{N_{11}}{t-s} \psi(t) dt = \frac{b(s+1)}{2R}, \quad |s| < 1,$$

$$(5.25) \quad \int_{-1}^1 \psi(s) ds = \frac{2P}{b}.$$

In this case α is positive and β is negative since the parabolic punch has a sharp corner at $X = 0$ and smooth contact at $X = b$. By letting $N_0 = 1$ and $M_0 = -1$, α and β are the same as those defined in Eq. (5.16) and the index is $\kappa_0 = 0$.

The left-hand side of Eq. (5.24) can be expanded into a series of Jacobi polynomials $P_j^{(-\alpha, -\beta)}(\cdot)$ [23]

$$(5.26) \quad \frac{b(s+1)}{2R} = \frac{b \left[P_1^{(-\alpha, -\beta)}(s) + (1+\alpha) P_0^{(-\alpha, -\beta)}(s) \right]}{2R}.$$

Substituting Eq. (4.17) into Eq. (5.24) in view of Eq. (5.26), using Eq. (4.20) and considering Eq. (5.5) yield the nonzero coefficient as follows:

$$(5.27) \quad c_0 = \frac{b(1+\alpha)}{-2N_{11}R} \sin(\pi\alpha), \quad c_1 = \frac{b}{-2N_{11}R} \sin(\pi\alpha).$$

Thus, by considering Eqs. (4.17), (4.10) and (2.7), one can get the surface normal stress as

$$(5.28) \quad \sigma_{YY}(X, 0) = \frac{b \sin(\pi\alpha)}{N_{11}R} \left(\frac{b-X}{X} \right)^\alpha \left(\alpha + \frac{X}{b} \right), \quad 0 < X < b.$$

The surface in-plane stress given in Eq. (4.6) can be rewritten in the following closed-form:

$$(5.29) \quad \sigma_{XX}(X, 0) = \frac{b \sin(\pi\alpha)}{-N_{11}R} \times \begin{cases} N_{21} \left(\frac{b-X}{X} \right)^\alpha \left(\alpha + \frac{X}{b} \right) + \frac{N_{22} \cdot \mu_f}{2\pi} [(1+\alpha)\Upsilon_p^{(0)}(X) + \Upsilon_p^{(1)}(X)], & 0 < X < b, \\ \frac{N_{22} \cdot \mu_f}{2\pi} [(1+\alpha)\Upsilon_p^{(0)}(X) + \Upsilon_p^{(1)}(X)], & X < 0, X > b, \end{cases}$$

where

$$(5.30) \quad \Upsilon_p^{(0)}(X) = \frac{\pi}{\sin(\pi\alpha)} \begin{cases} \left(\frac{X-b}{X} \right)^\alpha - 1, & X < 0, \\ \left(\frac{b-X}{X} \right)^\alpha \cos(\pi\alpha) - 1, & 0 < X < b, \\ \left(\frac{X-b}{X} \right)^\alpha - 1, & X > b, \end{cases}$$

$$(5.31) \quad \Upsilon_p^{(1)}(X) = P_1^{(\alpha, \beta)} \left(\frac{2X}{b} - 1 \right) \Upsilon_p^{(0)}(X) + \frac{2\pi\alpha}{\sin(\pi\alpha)}.$$

Substituting Eq. (4.17) into Eq. (5.25) in view of Eqs. (5.27) and (4.16) yields the following formula to determine the unknown contact length:

$$(5.32) \quad b = \sqrt{\frac{-2 \cdot N_{11} \cdot P \cdot R}{\pi \cdot \alpha \cdot (1 + \alpha)}}.$$

Then, the mode I stress intensity factor at the edge $X = 0$ of the parabolic punch can be defined as

$$(5.33) \quad F_I(0) = \lim_{X \rightarrow 0} X^\alpha p(X) = \frac{b^{\alpha+1} \cdot \alpha \cdot \sin(\pi\alpha)}{-N_{11} \cdot R}.$$

Letting $\mu_f = 0$ leads to

$$(5.34) \quad F_I(0) = b^{\frac{3}{2}} / (-2 \cdot N_{11} \cdot R).$$

5.4. For a frictional cylindrical punch

In this case, considering the fourth expression on the left-hand side of Eq. (2.6), one can rewrite Eqs. (4.8) and (4.9) as

$$(5.35) \quad N_{12} \cdot \mu_f \cdot \psi(s) + \frac{1}{\pi} \int_{-1}^1 \frac{N_{11}}{t-s} \psi(t) dt = \Lambda(s) = \frac{(b+a)s + b-a}{2R}, \quad |s| < 1,$$

$$(5.36) \quad \int_{-1}^1 \psi(r) dr = \frac{2P}{a_0},$$

where

$$(5.37) \quad a_0 = b + a, \quad a_1 = b - a.$$

In this case α and β are positive since the cylindrical punch has smooth contacts both at $X = -a$ and $X = b$. By letting $N_0 = 1$ and $M_0 = 0$, α and β defined in Eq. (4.18) can be obtained as

$$(5.38) \quad \begin{aligned} \xi > 0: \quad \alpha &= 1 - \frac{\xi}{\pi}, & \beta &= \frac{\xi}{\pi}, \\ \xi = 0: \quad \alpha &= \frac{1}{2}, & \beta &= \frac{1}{2}, \\ \xi < 0: \quad \alpha &= \frac{\xi}{\pi}, & \beta &= 1 - \frac{\xi}{\pi}. \end{aligned}$$

Thus, the index κ_0 in this case is

$$(5.39) \quad \kappa_0 = -(\alpha + \beta) = -1.$$

Due to $\kappa_0 = -(\alpha + \beta) = -1$, the following consistency condition must be fulfilled:

$$(5.40) \quad \int_{-1}^1 \frac{\Lambda(s)}{\varpi(s)} ds = 0.$$

Expanding the left-hand side of Eq. (5.35) into the following series of Jacobi polynomials $P_j^{(-\alpha, -\beta)}(\cdot)$ [23]:

$$(5.41) \quad \begin{aligned} & [(b+a)s + b-a]/(2R) \\ &= \{2a_0 P_1^{(-\alpha, -\beta)}(s) + [a_1 - (\beta - \alpha)a_0] P_0^{(-\alpha, -\beta)}(s)\}/2R, \end{aligned}$$

and comparing both sides of Eq. (4.20) in view of Eq. (5.5), one arrives at the only nonzero coefficient

$$(5.42) \quad c_0 = \frac{a_0}{-2N_{11}R} \sin(\pi\alpha) = \frac{b+a}{-2N_{11}R} \sin(\pi\alpha).$$

Thus, with consideration of Eqs. (4.17), (4.10) and (2.7), the surface normal stress can be obtained as

$$(5.43) \quad \sigma_{YY}(X, 0) = \frac{\sin(\pi\alpha)}{N_{11}R} (b-X)^\alpha (X+a)^\beta, \quad -a < X < b.$$

The surface in-plane stress given in Eq. (4.6) can be rewritten in the following closed-form:

$$(5.44) \quad \sigma_{XX}(X, 0) = \frac{\sin(\pi\alpha)}{-N_{11}R} \begin{cases} N_{21}(b-X)^\alpha (X+a)^\beta + \frac{N_{22} \cdot \mu_f}{2\pi} \Upsilon_c(X), & -a < X < b, \\ \frac{N_{22} \cdot \mu_f}{2\pi} \Upsilon_c(X), & X \notin [-a, b], \end{cases}$$

where $\Upsilon_c(X)$ is given as

$$(5.45) \quad \Upsilon_c(X) = \frac{\pi}{\sin(\pi\alpha)} \times \begin{cases} -2(b-X)^\alpha (-X-a)^\beta - 2X + b - a + (\alpha - \beta)(b+a), & X < -a, \\ 2(b-X)^\alpha (X+a)^\beta - 2X + b - a + (\alpha - \beta)(b+a), & -a < X < b, \\ 2(X-b)^\alpha (X+a)^\beta - 2X + b - a + (\alpha - \beta)(b+a), & X > b. \end{cases}$$

By considering Eqs. (5.42) and (4.16) and using the equilibrium equation (5.36) yield the relationship between the load and the contact length

$$(5.46) \quad P = \frac{\pi \cdot \alpha \cdot \beta}{-2N_{11} \cdot R} (b+a)^2.$$

Applying the consistency condition given in Eq. (5.40), one has the following relationship to determine the unknown contact length:

$$(5.47) \quad b = \frac{\beta}{\alpha} a.$$

In this section, analytical solution of the singular integral equation is obtained for punches with four different profiles; unconventional singularity, relationship between the indentation load and the contact length, and explicit expression of surface in-plane stress are presented.

6. Numerical results and discussions

For numerical computations, the corresponding material properties are given as follows: $C_{11} = 159.7885$ GPa, $C_{12} = 5.2609$ GPa, $C_{22} = 15.4732$ GPa and $G_0 = 5.52$ GPa.

6.1. Eigenvalue distribution

Table 1 demonstrates the eigenvalue distribution with varying relative moving velocity. Frictional elastic dynamic contact can be unstable. As the relative moving velocity c increases, the following cases emerge: a) two pairs of opposite real roots, b) a pair of opposite real roots and a pair of purely imaginary roots, and c) two pairs of purely imaginary roots. In view of the regularity conditions given in Eq. (2.11), instability occurs. Only case a, i.e., two pairs of opposite real roots, is practicable for the semi-infinite composite. Thus, the c values are chosen within the interval $[0, 1)$ in the numerical computation. It is noted that though even the value of the parameter $c = 0.1$ corresponds to the value of velocity about $V \gg 100$ m/s, the motion should be subsonic, i.e., the moving speed V should not exceed the lowest bulk wave velocity $c_B = \sqrt{C_{33}\rho}$.

Table 1. Eigenvalue distribution with relative moving velocity ($i^2 = -1$).

c	η_1	η_2	η_3	η_4
0	5.2506	-5.2506	0.6120	-0.6120
0.1	5.2496	-5.2496	0.6090	-0.6090
0.2	5.2468	-5.2468	0.5997	-0.5997
0.3	5.2421	-5.2421	0.5839	-0.5839
0.4	5.2356	-5.2356	0.5610	-0.5610
0.5	5.2271	-5.2271	0.5301	-0.5301
0.6	5.2168	-5.2168	0.4897	-0.4897
0.7	5.2045	-5.2045	0.4372	-0.4372
0.8	5.1904	-5.1904	0.3674	-0.3674
0.9	5.1743	-5.1743	0.2669	-0.2669
1	0	0	5.1562	-5.1562
1.5	5.0359	-5.0359	0.6852i	-0.6852i
2	4.8626	-4.8626	1.0626i	-1.0626i
10	8.5829i	-8.5829i	5.8365i	-5.8365i

6.2. Surface in-plane stress under a frictional flat punch

Figure 1 shows the effects of the relative moving velocity c and the friction coefficient μ_f on the normalized surface in-plane stress $\sigma_{XX}(X, 0)/\sigma_0$

($\sigma_0 = P/2a$) under a frictional flat punch. The surface in-plane stress is unbounded and discontinuous at both the trailing edge and the leading edge of the flat punch. The stress concentrations of the surface in-plane stress may explain why the surface damage occurs under the action of the flat punch. When the flat punch moves frictionally, the surface in-plane stress is compressive before the trailing edge ($X < a$), while tensile behind the trailing edge ($X > a$), which agrees with the well-known experimental findings that the trailing edge has a great potential to be a location of the surface crack initiation and propagation in load transfer components [24].

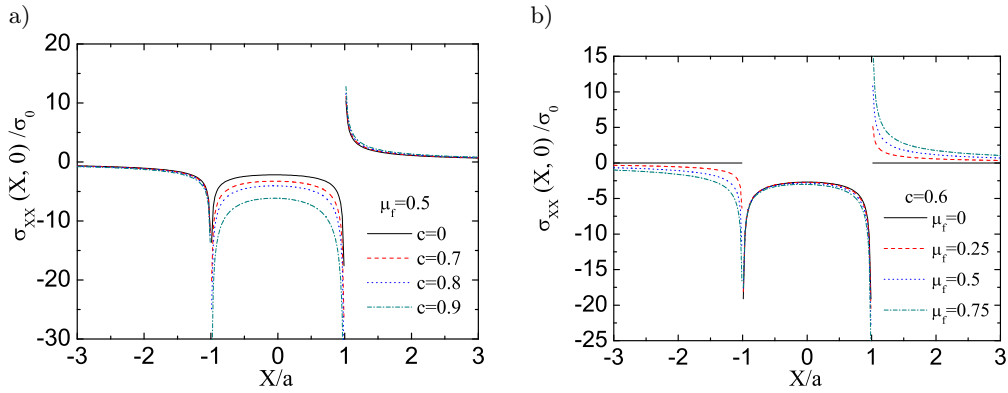


FIG. 1. The effects of: a) the relative moving velocity c and b) the friction coefficient μ_f on the normalized surface in-plane stress $\sigma_{XX}(X, 0)/\sigma_0$ ($\sigma_0 = P/2a$) under a frictional flat punch.

In addition, Fig. 1a presents the situation that when the flat punch moves faster, the magnitudes of the surface in-plane stress intensify inside the contact region, while they keep almost the same values outside the contact region.

Figure 1b depicts the scenario that when the sliding contact interface becomes more frictional, the surface in-plane stress beneath the punch ($|X| < a$) intensifies around the trailing edge of the punch. With the increasing of friction coefficient, the surface in-plane stress becomes more tensile behind the trailing edge ($X > a$), while more compressive before the leading edge ($X < -a$).

It seems that the friction coefficient μ_f has a more significant influence on the surface in-plane stress than the relative moving velocity c does when under the action of the flat punch.

6.3. Surface in-plane stress under a frictional triangular punch

Figure 2 delineates the influences of the relative moving velocity c and the friction coefficient μ_f on the normalized surface in-plane stress $\sigma_{XX}(X, 0)/\sigma_0$ ($\sigma_0 = -m_0/N_{11}(0)$, where $N_{11}(0)$ is the value of N_{11} when $c = 0$) under a fric-

tional triangular punch. The surface in-plane stress $\sigma_{XX}(X, 0)/\sigma_0$ is discontinuous around the edge $X = 0$, while it has a tensile spike for nonzero values of the friction coefficient μ_f at the edge $X = b$. The tensile spike as $X \rightarrow b$ under a triangular punch has a relevance to the well-known experimental findings that the surface crack initiation and propagation in load transfer components more likely occur at the trailing edge [24].

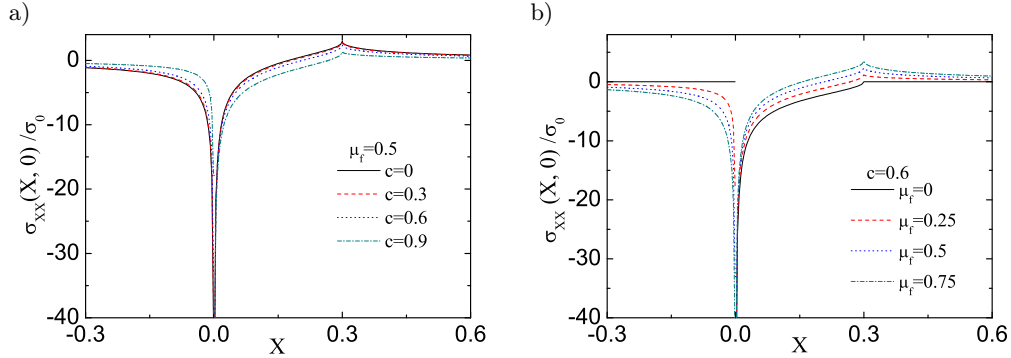


FIG. 2. The effects of: a) the relative moving velocity c and b) the friction coefficient μ_f on the normalized surface in-plane stress $\sigma_{XX}(X, 0)/\sigma_0$ ($\sigma_0 = -m_0/N_{11}(0)$) under a frictional triangular punch.

In addition, Fig. 2a shows that the relative moving velocity c has no that pronounced influence on the surface in-plane stress under the triangular punch. Figure 2b illustrates that the tensile spike of the surface in-plane stress increases with the friction coefficient μ_f increasing. The magnitude of the surface in-plane stress around the edge $X = 0$ decreases as the friction coefficient μ_f increases when $X > 0$; while the opposite trend can be observed when $X < 0$.

The stress concentration of surface in-plane stress around the edge $X = 0$ and spike of the surface in-plane stress at the edge $X = b$ may explain why the surface damage occurs under the action of the triangular punch.

6.4. Surface in-plane stress under a frictional parabolic punch

Figure 3 demonstrates the influences of the relative moving velocity c and the friction coefficient μ_f on the normalized surface in-plane stress $\sigma_{XX}(X, 0)/\sigma_0$ ($\sigma_0 = P/R$) under a frictional parabolic punch. The surface in-plane stress $\sigma_{XX}(X, 0)/\sigma_0$ is discontinuous around the edge $X = 0$, while it has a tensile spike for nonzero values of the friction coefficient μ_f at the edge $X = b$. These phenomena are the same as those under the triangular punch. The tensile spike as $X \rightarrow b$ under a parabolic punch reaffirms that the surface crack initiation and propagation in load transfer components more likely happen at the trailing edge [24].

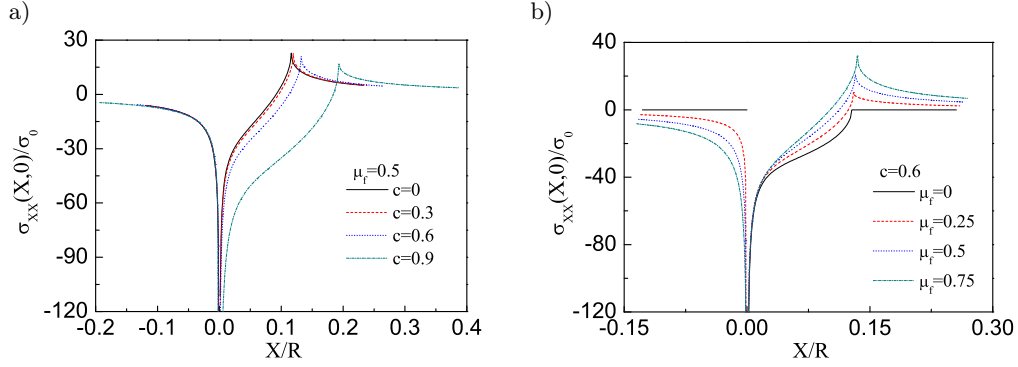


FIG. 3. The effects of: a) the relative moving velocity c and b) the friction coefficient μ_f on the normalized surface in-plane stress $\sigma_{XX}(X,0)/\sigma_0$ ($\sigma_0 = P/R$) under a frictional parabolic punch.

In addition, Fig. 3 shows that the tensile spike at the edge $X = a$ increases with either the relative moving velocity decreasing or the friction coefficient increasing.

Like the triangular punch case, the stress concentration of the surface in-plane stress and spike of the surface in-plane stress may explain why surface damage occurs under the action of the parabolic punch.

6.5. Surface in-plane stress under a frictional cylindrical punch

Figure 4 illustrates the influences of the relative moving velocity c and the friction coefficient μ_f on the normalized surface in-plane stress $\sigma_{XX}(X,0)/\sigma_0$ ($\sigma_0 = P/R$) under a frictional cylindrical punch. The normalized surface in-plane stress $\sigma_{XX}(X,0)/\sigma_0$ has a tensile spike at the edge $X = b$ when $\mu_f > 0$, which may imply the initiation and sub-critical growth of surfaces crack under

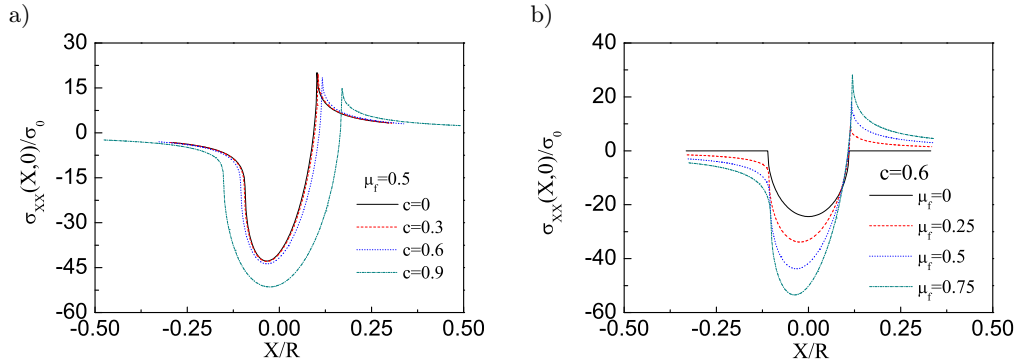


FIG. 4. The effects of: a) the relative moving velocity c and b) the friction coefficient μ_f on the normalized surface in-plane stress $\sigma_{XX}(X,0)/\sigma_0$ ($\sigma_0 = P/R$) under a frictional cylindrical punch.

repeated loadings and confirms the well-known experimental findings [24] like those under a triangular or parabolic punch.

With the relative moving velocity c increasing, the spike value of surface in-plane stress at $X = b$ decreases and peak magnitude location becomes closer to the edge $X = -a$ as observed in Fig. 4a. Figure 4b demonstrates that with the friction coefficient μ_f increasing, the spike value of surface in-plane stress at $X = b$ increases and peak magnitude location becomes closer to the edge $X = -a$.

The spike of in-plane stress may explain why surface damage occurs under the action of the cylindrical punch.

7. Conclusions

A general theory on orthotropic materials under a moving rigid punch is set up. The punch moves to the right or left at a constant speed. The Coulomb friction law is modeled inside the contact region. Galilean transformation and Fourier transform are applied to obtain the appropriate fundamental solutions, which can lead to real expressions of physical quantities in case of either real or complex eigenvalues. Through an asymptotic analysis of the kernels, singular integral equations of the second kind in terms of unknown contact stress beneath the punch are obtained. Explicit formulae of various surface stresses are obtained for four cases, including flat, triangular, parabolic and cylindrical punch, and non-classical singularity is presented.

Numerical results show that the relative moving velocity affects the eigenvalue distribution, while the friction coefficient does not. The influences of relative moving velocity and the friction coefficient on the surface in-plane stress are revealed in each case of the four types of punches, which delineate that the surface crack initiation and propagation in load transfer components are more likely to occur at the trailing edge.

Appendix

1. Expressions of $\Omega_{mn}(\zeta, Y)$ ($m = 1, 2, 3$, $n = 1, 2$) appearing in Eq. (3.7):

Case A

$$(A.1) \quad \begin{aligned} \Omega_{m1}(\zeta, Y) &= [\Delta_{m1} \cos(|\zeta| \vartheta Y) - \Delta_{m2} \sin(|\zeta| \vartheta Y)] e^{|\zeta| \theta Y}, \\ \Omega_{m2}(\zeta, Y) &= [\Delta_{m2} \cos(|\zeta| \vartheta Y) + \Delta_{m1} \sin(|\zeta| \vartheta Y)] e^{|\zeta| \theta Y}, \end{aligned}$$

where Δ_{mn} ($m = 1, 2, 3$, $n = 1, 2$) are given as

$$(A.2) \quad \begin{aligned} \Delta_{11} &= -i \cdot \operatorname{sgn}(\zeta) \{C_{11} + C_{12} [\theta \cdot \operatorname{Re}(h(\eta_1)) - \vartheta \cdot \operatorname{Im}(h(\eta_1))]\}, \\ \Delta_{12} &= -i \cdot \operatorname{sgn}(\zeta) C_{12} [\theta \cdot \operatorname{Im}(h(\eta_1)) + \vartheta \cdot \operatorname{Re}(h(\eta_1))], \end{aligned}$$

$$\begin{aligned}
(A.3) \quad \Delta_{21} &= -i \cdot \operatorname{sgn}(\zeta) \{C_{12} + C_{22} [\theta \cdot \operatorname{Re}(h(\eta_1)) - \vartheta \cdot \operatorname{Im}(h(\eta_1))]\}, \\
\Delta_{22} &= -i \cdot \operatorname{sgn}(\zeta) C_{22} [\theta \cdot \operatorname{Im}(h(\eta_1)) + \vartheta \cdot \operatorname{Re}(h(\eta_1))], \\
(A.4) \quad \Delta_{31} &= C_{33} [\theta - \operatorname{Re}(h(\eta_1))], \\
\Delta_{32} &= C_{33} [\vartheta - \operatorname{Im}(h(\eta_1))].
\end{aligned}$$

Case B

$$(A.5) \quad \Omega_{mn}(\zeta, Y) = O_{mn} e^{|\zeta| \delta_n Y},$$

where O_{mn} ($m = 1, 2, 3$, $n = 1, 2$) are given as

$$(A.6) \quad O_{1n} = -i \cdot \operatorname{sgn}(\zeta) [C_{11} + C_{12} \delta_n h(\delta_n)],$$

$$(A.7) \quad O_{2n} = -i \cdot \operatorname{sgn}(\zeta) [C_{12} + C_{22} \delta_n h(\delta_n)],$$

$$(A.8) \quad O_{3n} = C_{33} [\delta_n - h(\delta_n)].$$

2. Expressions of M_{mn} ($m, n = 1, 2$) appearing in Eq. (4.4):

$$(A.9) \quad M_{11} = \frac{\Omega_{32}(\zeta, 0)}{\Omega_{21}(\zeta, 0)\Omega_{32}(\zeta, 0) - \Omega_{31}(\zeta, 0)\Omega_{22}(\zeta, 0)},$$

$$M_{12} = \frac{\Omega_{22}(\zeta, 0)}{\Omega_{21}(\zeta, 0)\Omega_{32}(\zeta, 0) - \Omega_{31}(\zeta, 0)\Omega_{22}(\zeta, 0)},$$

$$(A.10) \quad M_{21} = \frac{\Omega_{31}(\zeta, 0)}{\Omega_{21}(\zeta, 0)\Omega_{32}(\zeta, 0) - \Omega_{31}(\zeta, 0)\Omega_{22}(\zeta, 0)},$$

$$M_{22} = \frac{\Omega_{21}(\zeta, 0)}{\Omega_{21}(\zeta, 0)\Omega_{32}(\zeta, 0) - \Omega_{31}(\zeta, 0)\Omega_{22}(\zeta, 0)}.$$

Acknowledgments

This work was supported by the National Natural Science Foundation of China (11090334, 11362018 and 11261045) and the Fundamental Research Funds for the Central Universities (1330219140).

References

1. S. SAMPATH, H. HERMAN, N. SHIMODA, T. SAITO, *Thermal spray processing of FGMs*, MRS Bulletin, **20**, 27–31, 1995.
2. W.A. KAYSSER, B. ILSCHNER, *FGM research activities in Europe*, MRS Bulletin, **20**, 22–26, 1995.

3. L.A. GALIN, *Contact problems in the theory of elasticity*, Gostekhizdat, Moscow, 1953; English transl.: 1961.
4. G.M. GLADWELL, *Contact Problems in the Classical Theory of Elasticity*, Kluwer Academic Publishers, Dordrecht, 1980.
5. K.L. JOHNSON, *Contact Mechanics*, Cambridge University Press, London, 1985.
6. D.A. HILLS, D. NOWELL, A. SACKFIELD, *Mechanics of Elastic Contacts*, Butterworth-Heinemann, Oxford, 1993.
7. D. SHI, Y. LIN, T.C. OVAERT, *Indentation of an orthotropic half-space by a rigid ellipsoidal indenter*, Journal of Tribology, **125**, 223–231, 2003.
8. S.R. SWANSON, *Hertzian contact of orthotropic materials*, International Journal of Solids and Structures, **41**, 1945–1959, 2004.
9. S.R. SWANSON, *Contact deformation and stress in orthotropic plates*, Composites: Part A, **36**, 1421–1429, 2005.
10. G. LYKOTRAFITIS, H.G. GEORGIADIS, P.A. GOURGIOTIS, *Rapid sliding motion of a rigid frictionless indenter with a flat base over a thermoelastic half-space*, Archive of Applied Mechanics, **82**, 1481–1495, 2012.
11. J.W. CRAGGS, A.M. ROBERTS, *On the motion of a heavy cylinder over the surface of an elastic solid*, ASME Journal of Applied Mechanics, **24**, 207–209, 1967.
12. D.L. CLEMENT, *On the motion of a heavy cylinder over the surface of an anisotropic elastic solid*, SIAM Journal on Applied Mathematics, **19**, 116–124, 1970.
13. H.G. GEORGIADIS, J.R. BARBER, *On the super-Rayleigh/subseismic elastodynamic indentation problem*, Journal of Elasticity, **31**, 141–161, 1993.
14. L.M. BROCK, *Exact analysis of dynamic sliding indentation at any constant speed on an orthotropic or transversely isotropic half-space*, ASME Journal of Applied Mechanics, **69**, 340–345, 2002.
15. J.R. BARBER, M. COMINON, *Rolling of elastic cylinders with friction at supersonic speed*, International Journal of Solids and Structures, **18**, 783–789, 1982.
16. L.M. BROCK, *Some analytical results for heating due to irregular sliding contact of thermoelastic solids*, Indian Journal of Pure and Applied Mathematics, **27**, 1257–1278, 1996.
17. L.M. BROCK, *Rapid sliding indentation with friction of a pre-stressed thermoelastic material*, Journal of Elasticity, **53**, 161–188, 1999.
18. L.M. BROCK, H.G. GEORGIADIS, *Sliding contact with friction on a thermoelastic solid at subsonic, transonic and supersonic speeds*, Journal of Thermal Stresses, **23**, 629–656, 2000.
19. L.M. BROCK, H.G. GEORGIADIS, *Multiple-zone sliding contact with friction on an anisotropic thermoelastic half-space*, Int. J. Solids & Structures **44**, 2820–2836, 2007.
20. Y.T. ZHOU, K.Y. LEE, Y.H. JANG, *Influences of the moving velocity and material property on frictionless contact problem of orthotropic materials indented by a moving punch*, Archives of Mechanics, **65**, 195–217, 2013.
21. N.I. MUSKHELISHVILI, *Singular Integral Equations*, P. Noordhoff, Groningen, 1953.

22. I.S. GRADSHTEYN, I.M. RYZHIK, *Tables of Integrals, Series, and Products*, 4th ed., Academic Press, New York, 1980.
23. F. ERDOGAN, *Complex Function Technique*, Academic Press, New York, 1975.
24. S. SURESH, M. OLSSON, A.E. GIANNAKOPOULOS, N.P. PADTURE, J. JITCHAROEN, *Engineering the resistance to sliding-contact damage through controlled gradients in elastic properties at contact surfaces*, *Acta Materialia*, **47**, 3915–3926, 1999.

Received June 28, 2013; revised version December 6, 2013.
